Generic Modeling of a Line Commutated Converter based Multi-Terminal HVDC System for Power System Stability Studies

Christoph Hahn, Thomas Schlegl,
Matthias Luther
Institute of Electrical Energy Systems
Friedrich-Alexander-University of Erlangen-Nuremberg
Erlangen, Germany
Christoph.Hahn@fau.de

Olaf Ruhle
Siemens Power Technologies International (PTI)
Siemens AG, Energy Management Division
Erlangen, Germany
Olaf.Ruhle@siemens.com

***Abstract* - This paper reveals a novel approach for generic modeling of a Line Commutated Converter (LCC) based Multi-Terminal (MT) High Voltage Direct Current (HVDC) system. The model is based on the mathematical correlations and appropriate transfer functions of a point-to-point connection; an expansion to a MT system is realized by the superposition of partial currents in the Multi-Terminal topology, which is easily applicable to a configuration with a large number of terminals.**

Furthermore the Combined and Coordinated Control Method (CCCM) is implemented in the model and investigated. Advantages and differences in the dynamic behavior compared to standard control approaches are carried out. By comparing the generic stability model with an EMT (Electro-Magnetic-Transient) HVDC model during a startup process and a subsequent AC voltage drop the consistence of the dynamic behavior is shown.

***Keywords* - HVDC Generic Modeling, HVDC Control Design, MTDC, LCC Control Methods, CCCM.**

I. INTRODUCTION

LCC based HVDC systems already exist for decades and are therefore well known and described e.g. in [1] - [3]. For bulk power transmission over long distances they are still the preferred solution since VSC technology is not capable of higher current ratings and AC technology is uneconomical for longer distances [4].

Recently, the desire to integrate HVDC systems into AC power systems has gained interest. E.g. Germany's national energy transition leads to the concept of building HVDC lines from northern to southern Germany according to the German Grid Development Plan [5]. In [6] and [7] conceptual studies for a European super grid, which could enhance the transmission of power from renewable energy sources, are provided. These systems are planned to be built in self commutated VSC technology. The majority of the existing MT systems – e.g. the Quebec-New England and the Italy-Corsica-Sardinia HVDC, which are in operation for more than 20 years [8] – comprise LCC technology. A new LCC based Multi-Terminal network will be built in India between the hydroelectric power plants in Biswanath, Chariali, Kishanganj and the City of Agra, where commissioning is planned for 2016 [9].

Currently existing Multi-Terminal systems are built in a parallel structure as exemplarily depicted in Fig. 1 and a maximum of three terminals are connected. In parallel structures, the current is used to control the transmitted power, while the voltage is nearly constant at every converter and only the voltage drop over the line causes differences.

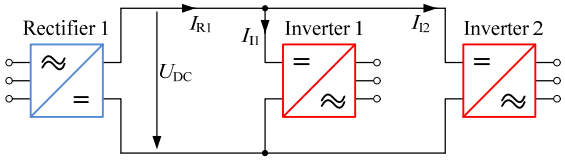

Fig. 1: Basic scheme of a three terminal parallel HVDC converter arrangement

A step further in this development is the application of meshed DC grids, which offer multiple routes for the power flow and grant a higher flexibility and more service security [10].

Generic stability models for LCC based HVDC systems, which are based on the system transfer functions, have been carried out e.g. in [11] and [12] . Multi-Terminal LCC based HVDC systems are introduced in [13], but detailed mathematical modeling approaches of these systems are not well known.

Control strategies and concepts for LCC based MT HVDC systems have not been intensively investigated either, since there are only a few concepts existing [14] - [16]. Newer concepts usually do not investigate pure LCC HVDC systems; for instance in [17] a control study of a hybrid system is performed and [18] cares especially about the integration of large onshore windfarms in LCC MT systems.

This paper reveals a novel modeling approach using the

978-1-4673-8848-1/16/$31.00 ©2016 IEEE

superposition of partial currents in the Multi-Terminal DC (MTDC) network in section II. In Section III a modern control strategy for LCC based HVDC systems – the Combined and Coordinated Control Method (CCCM) – is investigated. Simulation results, which include a comparison of the developed stability model with an EMT model, comprise a startup process of the HVDC system and a subsequent voltage drop; they are presented in chapter IV.

II. HVDC Modeling

The generic stability model is based on the calculation of the average DC voltage during one converter period and the transfer function of the DC system; it neglects the converter switching behavior as it might be used for power system stability studies and the converter switching is therefore not of interest. At the beginning, the basic modeling approach of a point-to-point system and the extension to a three and four terminal system is carried out. Afterwards a novel modeling approach for larger Multi-Terminal systems, using the superposition of partial DC currents, is determined.

A. Basic HVDC modeling

The structure of a six-pulse, two terminal HVDC system is presented in Fig. 2. Where X_{CR1} und X_{CI1} are the short circuit reactances of the converter transformers, V_{LLR1} and V_{LLI1} are the AC voltages of the transformer secondary side. f_{R1} and f_{I1} are the frequencies of the corresponding AC grids and V_{R1} and V_{I1} are the DC voltages at the converter stations. $I_{R1/I1}$ is the direct current, L_d and R_d are representing the DC line impedance.

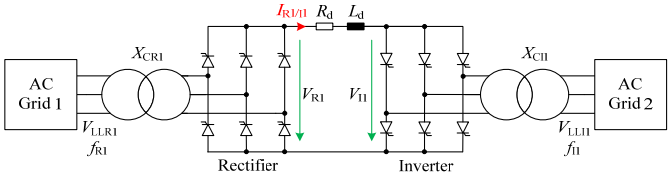

Fig. 2: Schematic layout of a six-pulse point-to-point HVDC system

The direct voltage at a converter can be calculated for a rectifier with (1) and for an inverter with (2) [1].

$$V_{R1} = B\frac{3\sqrt{2}}{\pi}\cdot V_{LLR1}\cos\alpha_{R1} - B\frac{3}{\pi}X_{CR1}I_{R1} \tag{1}$$

$$V_{I1} = B\frac{3\sqrt{2}}{\pi}\cdot V_{LLI1}\cos\gamma_{I1} - B\frac{3}{\pi}X_{CI1}I_{I1} \tag{2}$$

Where α is the firing angle, γ is the extinction angle and the parameter $B = 1$ for six-pulse HVDC systems and $B = 2$ for twelve-pulse units. Since α is the control variable at the inverter, γ has to be replaced with α in equation (2). Taking the correct sign of the direct current and the voltage drop due to the commutation into account, equation (3) can be stated.

$$V_{I1} = -B\frac{3\sqrt{2}}{\pi}\cdot V_{LLI1}\cos\alpha_{I1} + B\frac{3}{\pi}X_{CI1}I_{I1} \tag{3}$$

The differential equation of the simplified DC transmission line, as illustrated in Fig. 2, is stated in (4).

$$V_{R1} - V_{I1} = I_{R1/I1}R_d + L_d\frac{d}{dt}I_{R1/I1} \tag{4}$$

If equation (4) is solved for the direct current and transferred into the Laplace domain, equation (5) is gained.

$$I_{R1/I1}(s) = \frac{V_{R1}(s) - V_{I1}(s)}{R_d + sL_d} \tag{5}$$

The direct current in the system mainly depends on the voltage difference at the converter stations. With equations (1) and (3) to (5) a point-to-point HVDC system can be modeled as shown in Fig. 3.

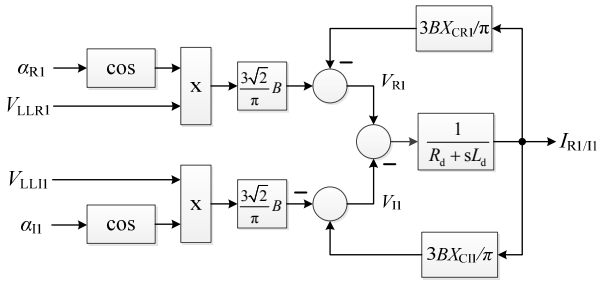

Fig. 3: Block diagram of a point-to-point HVDC system

The system of Fig. 2 is now extended by an inverter; the resulting network is illustrated in Fig. 4. In order to obtain the currents at the inverters in the network the equations (6) and (7) can be used. In contrast to a two terminal system there are different opportunities to gain an expression for the DC current at the inverters. The current at the rectifier – stated in equation (8) – is the superposition of (6) and (7).

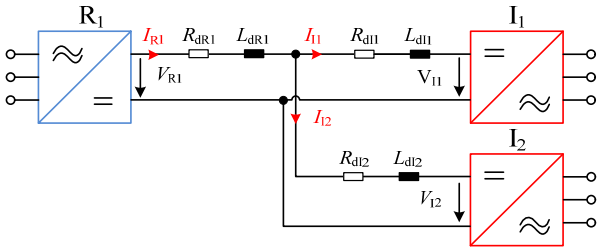

Fig. 4: Basic scheme of a three terminal system

$$I_{I1}(s) = \frac{V_{R1}(s) - V_{I1}(s) - I_{R1}(R_{dR1} + sL_{dR1})}{(R_{dI1} + sL_{dI1})} \tag{6}$$

$$I_{I2} = \frac{V_{R1}(s) - V_{I2}(s) - I_{R1}(R_{dR1} + sL_{dR1})}{(R_{dI2} + sL_{dI2})} \tag{7}$$

$$I_{R1}(s) = I_{I1}(s) + I_{I2}(s) \tag{8}$$

Using the equations (1) and (3) in order to obtain the DC voltages at the rectifier or the inverter respectively, and using the equations (6) to (8) for the determination of the DC currents, the block diagram of the three terminal system can be revealed, as depicted in in Fig. 5.

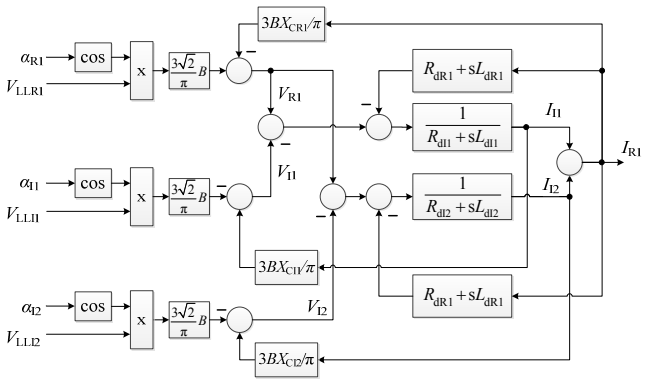

Fig. 5: Block diagram of a three terminal HVDC system

If the system is expanded by another rectifier, as shown in Fig. 6, there are even more opportunities to determine the direct currents in the system.

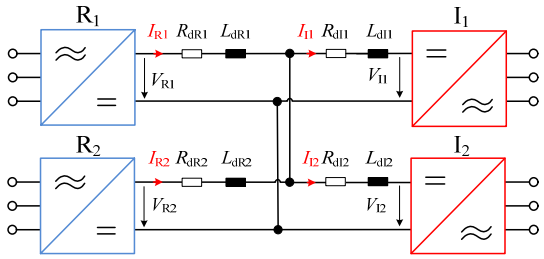

Fig. 6: Basic scheme of a four terminal system

If further converters would be added the complexity and effort of the calculation would rise continuously. Therefore, this method is insufficient in calculating complex networks in an efficient way. Instead, a new method to determine a mathematical model of a MT HVDC system is needed and explained in section B.

B. Modeling of Multi-Terminal HVDC systems using the superposition of partial currents

In Fig. 7 the basic idea of the principle is visualized applying a three terminal system according to Fig. 4. At first, the partial currents between the converters are calculated as it is done in a two terminal system. For a three terminal system, the current from the rectifier R1 to inverter I1 and subsequently the current from the rectifier R1 to the inverter I2 is determined as it is done for a point-to-point system. Hence, the current of the rectifier is the sum of the inverter currents. The appropriate impedances between the converter units are obtained by summarizing the resistances and reactances between the converters:

$$R_{\mathrm{dR1I1}} + \mathrm{s}L_{\mathrm{dR1I1}} = R_{\mathrm{dR1}} + R_{\mathrm{dI1}} + \mathrm{s}(L_{\mathrm{dR1}} + L_{\mathrm{dI1}}), \tag{9}$$

$$R_{\mathrm{dR1I2}} + \mathrm{s}L_{\mathrm{dR1I2}} = R_{\mathrm{dR1}} + R_{\mathrm{dI2}} + \mathrm{s}(L_{\mathrm{dR1}} + L_{\mathrm{dI2}}). \tag{10}$$

Thus, the partial currents of the system can be stated:

$$I_{\mathrm{R1I1}}(\mathrm{s}) = \frac{V_{\mathrm{R1}}(\mathrm{s}) - V_{\mathrm{I1}}(\mathrm{s})}{R_{\mathrm{R1I1}} + \mathrm{s}L_{\mathrm{R1I1}}}, \tag{11}$$

$$I_{\mathrm{R1I2}}(\mathrm{s}) = \frac{V_{\mathrm{R1}}(\mathrm{s}) - V_{\mathrm{I2}}(\mathrm{s})}{R_{\mathrm{R1I2}} + \mathrm{s}L_{\mathrm{R1I2}}}. \tag{12}$$

And the rectifier current reveals as:

$$I_{\mathrm{R1}}(\mathrm{s}) = I_{\mathrm{R1I1}}(\mathrm{s}) + I_{\mathrm{R1I2}}(\mathrm{s}). \tag{13}$$

Using the equations (11) to (13) the block diagram can be derived as shown in Fig. 7.

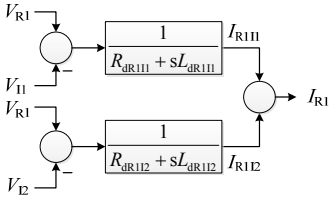

Fig. 7: Superposition of partial DC currents in a three terminal system

If the system is expanded to a four terminal system according to Fig. 6, the resulting impedances are determined as shown in equation (14), where $i \in \{1,2\}$ and $k \in \{1,2\}$. The determination of the partial currents of the four terminal system is shown in Fig. 8. As it can be seen, a partial current is defined as the contributing current of one rectifier-inverter-pair to the resulting converter current. There are two partial currents for every converter, since the system comprises two rectifiers and two inverters. The resulting currents at the converters are calculated as a superposition of the partial currents.

$$R_{\mathrm{dR}i\mathrm{I}k} + \mathrm{s}L_{\mathrm{dR}i\mathrm{I}k} = R_{\mathrm{dR}i} + R_{\mathrm{dI}k} + \mathrm{s}(L_{\mathrm{dR}i} + L_{\mathrm{dI}k}) \tag{14}$$

This approach can be extended to a Multi-Terminal system with an arbitrary number of rectifiers (n) and inverters (m); for this case, the calculation method of the rectifier and inverter currents is shown in Fig. 9 as a superposition of the respective partial currents. The appropriate impedances can again be calculated according to equation (14), where $i \in \{1,\ldots,\mathrm{n}\}$ and $k \in \{1,\ldots,\mathrm{m}\}$.

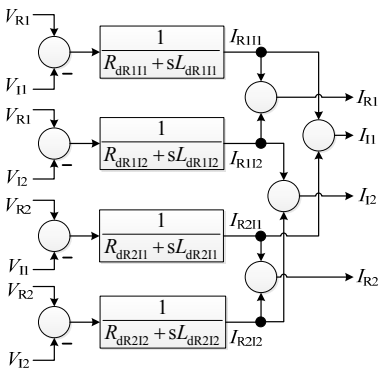

Fig. 8: Superposition of partial DC currents in a four terminal system

As illustrated in Fig. 9, the DC current of rectifier R1 is the superposition of the contributing partial currents of rectifier R1 connected to the respective inverters of the system (red sigma sign). The same principle applies for the inverters, as e.g. the DC current of inverter *m* is the superposition of the respective partial currents of the rectifiers connected to inverter *m* (green sigma sign). This approach provides a simple method to model MT HVDC systems with a large amount of converters.

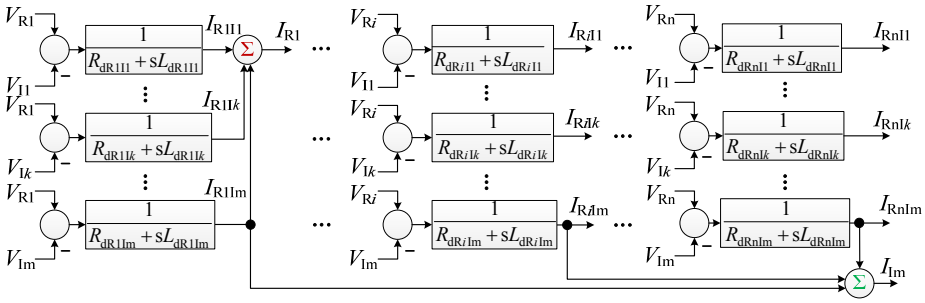

Fig. 9: Block diagram of a Multi-Terminal system with superposition of partial currents

C. Modeling of a meshed system with partial current approach

Considering a meshed MTDC system which consists of two rectifiers and two inverters, as shown in Fig. 10, the appropriate impedances of the system can be determined by applying equation (15). The red and green marked lines in Fig. 10 illustrate exemplarily the two possible ways of the power flow between rectifier R1 and inverter I1 and therefore the resulting impedance can be stated as a parallel circuit of the respective impedances.

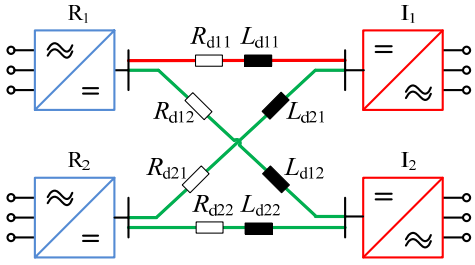

Fig. 10: Basic scheme of a meshed four terminal system

$$R_{\mathrm{dR}i\mathrm{I}k} + \mathrm{s}L_{\mathrm{dR}i\mathrm{I}k} = (R_{\mathrm{d}ik} + \mathrm{s}L_{\mathrm{d}ik}) \,\|\, \sum_{\substack{u,v=1 \\ u\neq i \wedge v\neq k}}^{2} (R_{\mathrm{d}uv} + \mathrm{s}L_{\mathrm{d}uv}) \qquad (15)$$

D. Grid connection via dynamic load

As the described model might be used for power system stability studies it needs to be connected to the AC grid. Therefore a dynamic load block – as this block is available in most of the simulation tools – can be used, where the active and reactive power are applied as input signals. The active power under the neglection of converter losses can be stated:

$$P = V_{\mathrm{R/I}} \cdot I_{\mathrm{R/I}}. \qquad (16)$$

In order to calculate the reactive power the overlap angle is needed. The overlap angle can be identified during a commutation cycle; solving the differential equations with the appropriate initial conditions yields [1]:

$$u = \arccos\left(\cos(\alpha) - \frac{2\omega I L_{CR/I}}{\sqrt{2}V_{LLR/I}}\right) - \alpha. \qquad (17)$$

Equation (18) describes the reactive power in dependence of the AC voltage, the DC current, the firing and overlap angle [1].

$$Q = \frac{3\sqrt{2}}{\pi} V_{\mathrm{LLR/I}} I_{\mathrm{R/I}} \frac{2u + \sin(2\alpha) - \sin\left(2(\alpha+u)\right)}{4\left(\cos\alpha - \cos(\alpha+u)\right)} \qquad (18)$$

III. Control Methods for MTDC

Up to now, LCC MT HVDC systems under operation use the Marginal Current Control Method (MCCM), which is described e.g. in [11]. Another control method for MT HVDC systems is the Combined and Coordinated Control Method (CCCM), which was invented by F. Karlecik-Maier [19]; detailed analyses can be found in [20]. The goal was to improve the dynamic behavior in case of disturbances and fault recovery. The CCCM has never been used in a commercial application, in spite of its advantages, especially for weak AC grids; therefore the CCCM will be applied and investigated in this paper.

Using this approach, the rectifiers directly control the active power which is transmitted via the DC link, where the following control function – which is also shown in Fig. 11 - applies:

$$\underbrace{\left(1 - \frac{I_{\mathrm{d}}}{I_{\mathrm{dref}}}\right)}_{di} + \underbrace{\left(1 - \frac{V_{\mathrm{d}}}{V_{\mathrm{dref}}}\right)}_{dv} = 0. \qquad (19)$$

The difference between the reference voltage level and actual voltage level, as well as the difference between the actual and reference current, is controlled. Once $V_{\mathrm{dref}} = V_{\mathrm{d}}$ and $I_{\mathrm{dref}} = I_{\mathrm{d}}$ equation (19) is complied, hence the reference power is transmitted and the controller is in steady state. By solving equation (19) for V_{d}, equation (20) is revealed.

$$V_{\mathrm{d}} = -\frac{V_{\mathrm{dref}}}{I_{\mathrm{dref}}} I_{\mathrm{d}} + 2V_{\mathrm{dref}} \qquad (20)$$

It can be seen, that equation (20) is the tangent on the hyperbola, which is revealed out of the power equation in the V-I-diagram in Fig. 12:

$$V_{\mathrm{d}} = \frac{P_{\mathrm{dref}}}{I_{\mathrm{d}}}. \qquad (21)$$

Using the CCCM, the inverters control a so-called equivalent resistance, where the following control function applies:

$$\underbrace{\left(1 - \frac{I_{\mathrm{d}}}{I_{\mathrm{dref}}}\right)}_{di} - \underbrace{\left(1 - \frac{V_{\mathrm{d}}}{V_{\mathrm{dref}}}\right)}_{dv} = 0. \qquad (22)$$

Solving this equation for the direct voltage yields in (23), which is a line through the origin in the V-I-diagram. Hence, it is representing an equivalent resistance.

$$V_d = \frac{V_{dref}}{I_{dref}} I_d \tag{23}$$

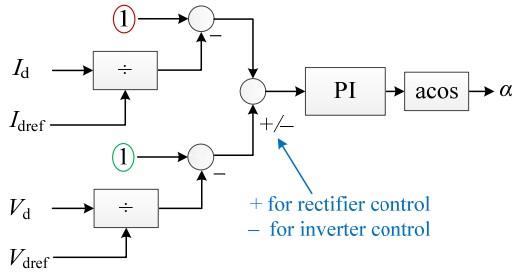

Fig. 11: CCCM control scheme at rectifier and Inverter respectively

The intersection of the tangent at the actual power in (20) and the equivalent resistance, as line through the origin in (23), is the stable operating point of the system. In Fig. 12 the V-I-characteristic of the CCCM is shown; the rectifier characteristics are highlighted in blue and the inverter characteristics in red. They are limited by applying maximum values for *dv* and *di*.

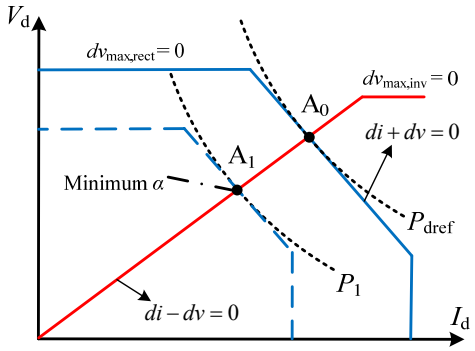

Fig. 12: Adjustment of the V-I-characteristic of the CCCM during an AC voltage drop at a rectifier

The steady state operating point, shown in Fig. 12, is A_0. If the AC voltage at the rectifier drops and the rectifier cannot compensate the voltage drop by increasing the firing angle, the DC voltage at the rectifier drops too. Since the control function of the rectifier applies as shown in equation (19), the current drops with the voltage and a new operating point is obtained at A_1.

Applying the CCCM to a MT HVDC system is a major advantage towards the MCCM, since in case of a voltage drop in the AC grid of a rectifier the control mode does not have to be changed. Applying the MCCM would cause the inverters to change from voltage to marginal DC current control mode, which might cause instabilities in the MT HVDC system.

Using the CCCM the reference DC voltage of the system is the maximum possible DC voltage of the weakest inverter. This leads to the necessity of communication between the converters. There are high requirements for transmission rate and reliability of the communication, which might be the reason why the CCCM has not been implemented in a real system yet.

IV. Results

The developed model and its appropriate control system, as described in the previous chapters, were implemented in MATLAB/Simulink® and PSS®NETOMAC. In order to verify the dynamic behavior of the developed mathematical stability model (index MSM), an EMT model was built up in MATLAB/Simulink® using the SimPowerSystems® Toolbox. The DC circuit configuration of Fig. 10 is used for the subsequent simulations. In order to compare both models, a startup process of the MT HVDC system and a subsequent AC voltage drop was performed, as depicted in Fig. 13 to Fig. 15, where Table I lists the most important parameters of the MT HVDC system and its appropriate control.

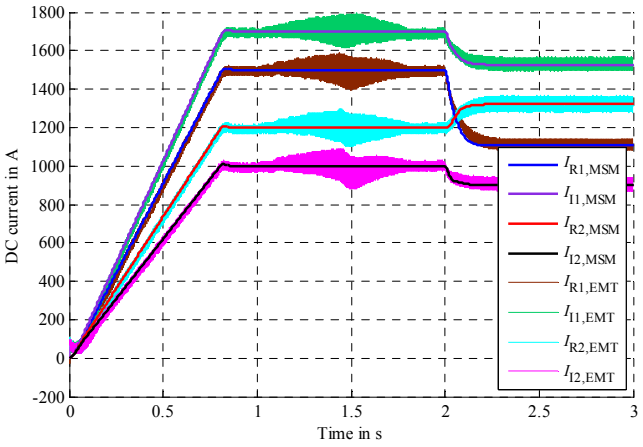

Fig. 13: DC currents of the MT HVDC models

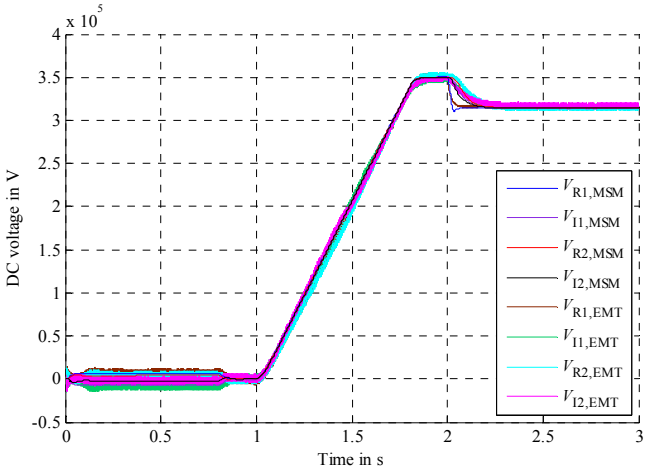

Fig. 14: DC voltages of the MT HVDC models

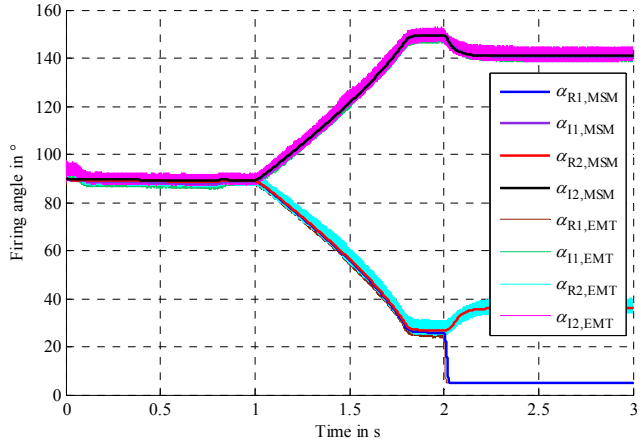

Fig. 15: Firing angles of the MT HVDC models

According to Fig. 11, at the beginning of the startup process the DC currents are increased; therefore the red marked 1 in the upper part of Fig. 11 is ramped up from 0 to 1, at the beginning of the simulation, with a time constant of 0.8 s. Once the DC currents have reached their steady state values, the green marked 1 in the lower part of Fig. 11 is ramped up from 0 to 1, at $t = 1$ s, with again a time constant of 0.8 s, and hence the DC voltages rise. The startup process of the entire MT HVDC system is finished after around 2 s and the system is in steady state. Using the CCCM, a very simple startup procedure of the MT HVDC system can be applied compared to other control approaches, where every converter needs an individual startup procedure.

After the startup process is performed, a 20% voltage drop in the AC grid of rectifier 1 is applied to the system, at $t = 2$ s. According to Fig. 12, the firing angle of the rectifier R1 reaches its limitation after the voltage drop and therefore the DC voltage of the system reaches a new steady state operating point, which is lower than the old one. The DC current of rectifier R1 decreases as described in chapter III and hence the new operating point, according to Fig. 12, is obtained. After the voltage drop, the HVDC system reaches a new steady state with a decreased power transmission.

Table I: System parameters

$V_{\mathrm{LLR/I}}$	300 kV	$X_{\mathrm{CR/I}}$	5.27 Ω
$f_{\mathrm{R/I}}$	50 Hz	B	1
V_{dref}	350 kV	$R_{\mathrm{d}uv}$	1.1 Ω
I_{dR1ref}	1500 A	$L_{\mathrm{d}uv}$	1.5 H
I_{dR2ref}	1200 A	K_{p}	0.4
I_{dI1ref}	1700 A	T_{N}	0.03 s
I_{dI2ref}	1000 A		

Fig. 13 to Fig. 15 show a very large and high conformity between the generic stability model and the EMT model. Only small deviations between the models can be found besides the deviations due to converter switching in the EMT model.

V. Conclusion

In this paper, a novel approach for modeling of LCC MT HVDC systems is derived. The approach uses the superposition of partial converter currents in order to obtain the appropriate DC currents; therefore the model is suitable for large MT HVDC networks, since the connection of further converters simply results in an addition of further partial currents. The model is developed with regard to simple system extendibility and can be easily adapted to VSC MT systems.

The Combined and Coordinated Control Method is applied to the model, as it is specially developed for controlling LCC MT HVDC systems. Using the CCCM, the active power of the system is controlled directly at the rectifiers and the inverters control an equivalent resistance.

Finally, the developed mathematical stability model is compared with an EMT model during a startup process and a subsequent AC voltage drop and a high conformity between the models could be figured out.

The model is implemented in MATLAB/Simulink® and PSS®NETOMAC, where the results of both simulation tools also show a high conformity; it can be used for comprehensive power system stability studies, as it comprises a detailed large signal model with its entire control scheme.

References

[1] E. W. Kimbark, *Direct Current Transmission*. John Wiley & Sons: New York, London, Sydney, Toronto, 1971.

[2] J. Arrillaga, *High Voltage Direct Current Transmission*. The Institution of Engineering and Technology: London (UK), 2008.

[3] K. R. Padiyar, *HVDC Power Transmission* Systems. New Academic Science Limited: Kent (UK), 2011.

[4] B. M. Buchholz, D. Povh and D. Retzmann, "Stability Analysis for large Power System Interconnections in Europe," in *Proc. IEEE Power Tech*, St. Petersburg, Russia, June 2005.

[5] 50Hertz Transmission, Amprion, TenneT TSO, TransnetBW – TSO's of Germany, "German grid development plan 2025 – 1st draft," (Netzentwicklungsplan Strom 2025 – Erster Entwurf), *The German Transmission System Operators*, Berlin, Germany, Oct. 2015.

[6] N. Ahmed, A. Haider, D. Van Hertem, L. Zhang and H.P. Nee, "Prospects and challenges of future HVDC SuperGrids with modular multilevel converters," in *Proc. IEEE European Power Electronics Conference*, Birmingham, United Kingdom, Aug. 2011.

[7] M. Callavik, J. Ahstrom and C. Yuen, "HVDC grids for continental wide power balancing," *10th international workshop on large scale integration of wind power into power system as well as on transmission networks for offshore wind power plants*, Aarhus, Denmark, Oct. 2011.

[8] R. P. Teixeira, *Multi-Terminal DC Networks.* CPI Koninkijke Wöhrmann: Delft, Zutphen, 2014.

[9] R. Nayak, R. Sasmal, V. Lescale, A. Kamur, C. Hong, H. Huang and N. Macloed, "Current status of design, engineering, manufacturing and testing of 800kV HVDC equipment," in *Proc. Cigre Second international symposium on standards for ultra high voltage transmission*, India, Jan. 2009.

[10] D. Jovcic, D. van Hertem, K. Linden, J.-P. Taisne and W. Grieshaber, "Feasibility of DC transmission networks," in *Proc. 2nd IEEE PES International Conference and Exhibition on Innovative Smart Grid Technologies (ISGT Europe)*, Manchester, Dec. 2011.

[11] C. Hahn, A. Semerow, M. Luther and O. Ruhle, "Generic Modeling of a Line Commutated HVDC System for Power System Stability Studies" in *Proc. IEEE PES T&D Conf. & Exp.*, Chicago, April 2014.

[12] R. M. Brandt, U. Annakkage, D. Brandt and N. Kshatriya, "Validation of a Two-Time Step HVDC Transient Stability Simulation Model including Detailed HVDC Controls and DC Line L/R Dynamics," *IEEE Power Engineering Society General Meeting*, Montreal, June 2006.

[13] J. Reeve, "Multiterminal HVDC Power Systems", in *IEEE Trans. Power App. Syst.*, Vol. 99, No. 2, April 1980.

[14] M. Han, H. Wang and X. Guo, "Control strategy research of LCC based multiterminal HVDC system", in *Proc. 2012 IEEE International Conference on Power System Technology (POWERCON)*, Auckland, Nov. 2012.

[15] K.R. Padiyar and Sachchidanad, "Stability of Converter Control of Multiterminal HVDC Systems", in *IEEE Trans. Power App. Systems*, Vol. PAS-104, No. 3, pp. 690-696, March 1985.

[16] T. Sakurai, K. Goto "A new control method for Multiterminal HVDC transmission without fast communication systems;" in *IEEE Trans. Power App. Syst.*, Vol. 102, No. 5, May 1983.

[17] O. Kotb, M. Ghandhari, R. Eriksson and V.K. Sood, "A study on the control of a hybrid MTDC system supplying a passive network," in *Proc. International Conference on Power System Technology (POWERCON)*, Chengdu, Oct. 2014.

[18] C. Xia, L. Weixing, S. Haishun, W. Jinyu, L. Naihu and Y. Liangzhong, "LCC based MTDC for grid integration of large onshore wind farms in Northwest China," in *Proc. IEEE Power and Energy Society General Meeting*, San Diego, July 2011.

[19] F. Karlecik-Maier, „A New Closed Loop Control Method for HVDC Transmission," in *IEEE Trans. Power Del.*, Vol.11, No.4, Oct. 1996

[20] P. Thepparat, *Analysis of the Combined and Coordinated Control Method for HVDC Transmission*, Aachen: Shaker Publishing, 2010.